

## Study of the $\pi^- \pi^+$ System in $\pi^- \pi^+ \pi^-$ Final States at COMPASS

---

**Fabian Krinner for the COMPASS collaboration\***

*Technische Universität München - Physik-Department - E18*

*E-mail: [fabian-krinner@mytum.de](mailto:fabian-krinner@mytum.de)*

The COMPASS experiment located at CERN's Super Proton Synchrotron is a multi-purpose fixed-target spectrometer aimed at studying the structure and spectrum of light hadrons using muon and hadron beams on various targets.

With its high acceptance and resolution, it has e.g. collected the world's biggest data set of diffractively produced  $\pi^- \pi^+ \pi^-$  final states. This large amount of data allows not only for a very detailed partial-wave analysis of this particular final state, but also for a new type of analysis which extracts the amplitude of the  $\pi^+ \pi^-$  subsystem with the quantum numbers  $I^G J^{PC} = 0^+ 0^{++}$  from the three-pion final state without any model input on its shape. This new study reveals correlations of the  $f_0(980)$  with decays of the  $\pi(1800)$ , the  $\pi_2(1880)$  as well as a new state, the  $a_1(1420)$ , which will be presented.

*52 International Winter Meeting on Nuclear Physics - Bormio 2014,  
27-31 January 2014  
Bormio, Italy*

---

\*Speaker.

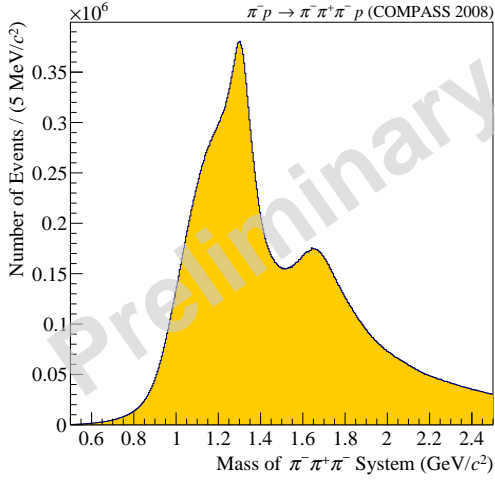


**Figure 1:** Invariant mass spectrum of the analyzed  $\pi^- \pi^+ \pi^-$  system.

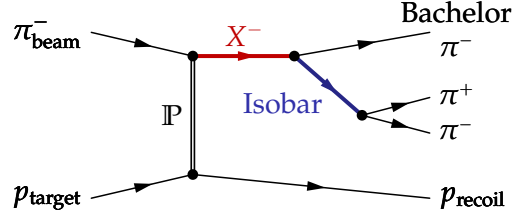


**Figure 2:** Diagrammatic view of the studied reaction. The  $\pi^- \pi^+ \pi^-$  final-state is diffractively produced via pomeron-exchange with the target-proton.

## 1. The COMPASS experiment

COMPASS, a multi-purpose fixed-target experiment, is located at CERN's Preveessin-area and supplied with various hadron and muon beams by the Super Proton Synchrotron. It is a two-stage high-resolution spectrometer with large acceptance that covers a wide kinematic range. Beam and final-state particles are identified via Cherenkov-detectors (CEDARs and RICH).

For the analysis presented here, data taken in 2008 are used. During this run, a 190 GeV negative secondary-hadron beam was used with a hydrogen target. This beam consists to 97% of  $\pi^-$ . The remaining part is mainly  $K^-$  and some  $\bar{p}$ .

## 2. The $\pi^- \pi^+ \pi^-$ final state

The work presented here analyzes the channel with three diffractively produced charged pions in the final state. During the 2008 run, about 50 million exclusive  $\pi^- \pi^+ \pi^-$  events were recorded, which constitutes at the moment by far the world's largest data sample for this particular channel.

### 2.1 Mass spectra

The three-pion invariant mass spectrum (Fig.1) of the selected events already shows a detailed structure due to several intermediate states. The most prominent features correspond to the well-established resonances  $a_1(1260)$ ,  $a_2(1320)$  and  $\pi_2(1690)$ . [1]

Looking at Dalitz plots for different three-pion masses  $m_{3\pi}$  also gives a first insight into the mass spectrum of the two-pion subsystem. Doing this at  $m_{3\pi}$  around 1.320 GeV and 1.670 GeV, which corresponds to the  $a_2(1320)$  and the  $\pi_2(1670)$ , respectively, reveals already a rich structure in the

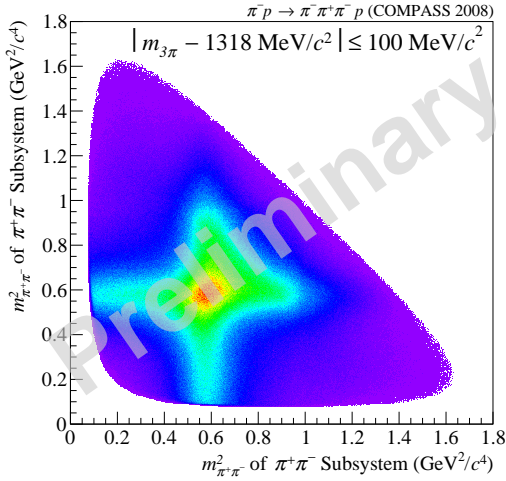


**Figure 3:** Dalitz plot for  $m_{3\pi}$  around the 1.320 GeV region, which is dominated by the well-known  $a_2(1320)$  resonance. In the plot, the also well-established  $\rho(770)$  is clearly visible.

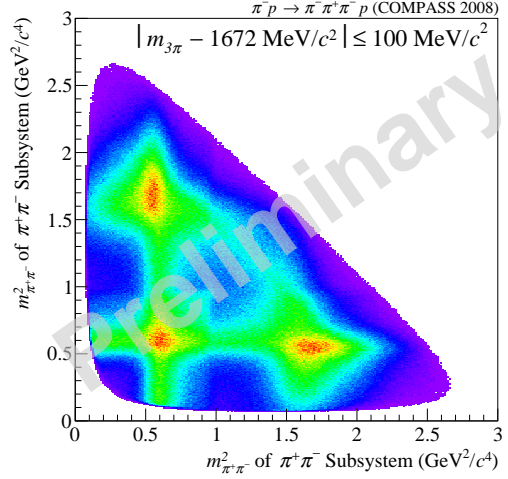


**Figure 4:** Dalitz plot for  $m_{3\pi}$  around the 1.670 GeV region, which is dominated by the  $\pi_2(1690)$  resonance. In the plot, the  $\rho(770)$  and the  $f_2(1270)$  are clearly visible. The sharp edge, seen around  $m_{\pi^-\pi^+} = 0.980$  GeV corresponds to the  $f_0(980)$  resonance.

two-pion mass,  $m_{\pi^-\pi^+}$ , that strongly depends on the chosen  $m_{3\pi}$ .

The structures, in the invariant mass spectra for  $m_{3\pi}$  and in the Dalitz plots for  $m_{\pi^-\pi^+}$  are disentangled further via more involved amplitude analysis techniques.

## 2.2 The isobar model

To get a further insight into the structure of the  $\pi^- \pi^+ \pi^-$  channel, some assumptions on the process have to be made. First, it is assumed, that the incoming  $\pi^-$  is excited via the exchange of a pomeron ( $\mathbb{P}$ ) with the target proton, and thus forms an intermediate state  $X^-$ . The pomeron hereby only carries four-momentum and spin, but neither charge nor isospin.

The second assumption is, that the intermediate state  $X^-$  does not decay directly into three charged pions, but undergoes a two-particle decay into a  $\pi^-$ , the bachelor pion, and another intermediate state, the so called isobar, which subsequently decays via a second two-particle decay into two pions, thus ending up in the  $\pi^- \pi^+ \pi^-$  final-state (see Fig.2). This assumption is known as the isobar-model.

## 3. Partial-wave analysis (PWA)

The invariant mass spectrum was analyzed via PWA in order to obtain further insight into the different contributions to the  $\pi^- \pi^+ \pi^-$  final state. The process is hereby described by a complex decay-amplitude, which is expanded into different intermediate states, called waves. These waves are defined by the quantum numbers of the intermediate state  $X^-$  as well as its decay products, the isobar and a  $\pi^-$  and their respective orbital angular momentum. This defines the angular distribution and shape in  $m_{\pi^-\pi^+}$  of the corresponding wave.

In contrast to Dalitz-plot analysis, PWA uses the full kinematic information in the data, and gives not only intensities for the different waves, but also information on their relative phases. This allows to clearly identify resonances, which not only show through peaks in the intensity, but also by their phase motion.

### 3.1 Established PWA method

In the PWA performed here, partial waves are defined in the following scheme:

$$J^{PC} M^\epsilon [\text{isobar}] \pi L. \quad (3.1)$$

The single quantum numbers are defined as follows:  $J$  gives the total spin of the wave,  $P$  and  $C$  its sign under parity and charge-conjugation, respectively,  $M$ , with  $M > 0$ , the magnetic quantum number of the wave and  $\epsilon$  the reflectivity. The isobar is given by a well-known  $\pi^- \pi^+$  resonance with specific quantum numbers, mass and width, and thus determines its shape in  $m_{\pi^- \pi^+}$  as well as the angular distribution of its subsequent decay into two pions. Finally,  $L$  gives the orbital angular momentum between the isobar and the bachelor pion.

In the PWA, six types of isobars were included: [1, 2]

$I^G J^{PC}$	
$0^+ 0^{++}$	$[\pi\pi]_S, f_0(980), f_0(1500)$
$1^+ 1^{--}$	$\rho(770)$
$0^+ 2^{++}$	$f_2(1270)$
$1^+ 3^{--}$	$\rho_3(1690)$

The  $[\pi\pi]_S$  listed above is also referred to as  $\sigma$ ,  $f_0(500)$  or  $f_0(600)$  in the literature.

For the current partial-wave analysis 87 of these waves up to a total spin of 6 were included. An incoherent isotropic wave describing uncorrelated events was also included. The final waveset was derived from an even larger set by successively removing waves that did not get any intensity by the fit.

### 3.2 Results of the PWA

For the results presented here, the fit to the data was performed in 20 MeV wide bins of the three-pion-mass, in a range from  $m_{3\pi} = 0.500 \text{ GeV}$  to  $2.500 \text{ GeV}$ , resulting in a total of 100 independent fits.

This PWA in mass bins is capable of describing the observed kinematic distribution very accurately. Its main features correspond to the  $a_1(1260)$ , the  $a_2(1320)$  and the  $\pi_2(1670)$  resonances in the dominant waves  $1^{++} 0^+ \rho(770) \pi S$ , the  $2^{++} 1^+ \rho \pi D$  and the  $2^{-+} 0^+ f_2(1270) \pi S$ , respectively (Figs.5, 6 and 7). [3] Besides these three waves, many other interesting waves are included in the PWA. For example the  $1^{-+} 1^+ \rho \pi P$  wave, where previous experiments claimed a spin-exotic resonance.

### 3.3 The $a_1(1420)$

In the PWA performed, also a new resonance-like structure is seen at  $1.4 \text{ GeV}$  in the  $1^{++} 0^+ f_0(980) \pi P$  wave. It has the same quantum numbers, as the well-known  $a_1(1260)$  resonance and thus is called

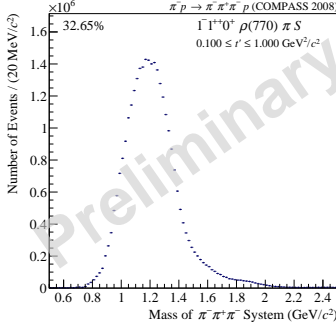


**Figure 5:** Intensity of the  $1^{++}0^+$   $\rho(770) \pi S$  wave. The  $a_1(1260)$  resonance can be clearly be seen.

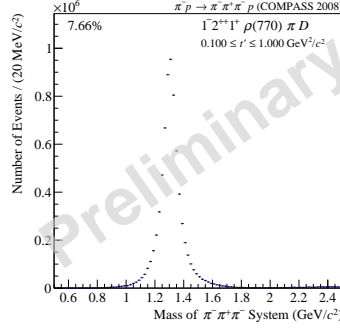


**Figure 6:** Intensity of the  $2^{++}1^+$   $\rho(770) \pi D$  wave. The  $a_2(1320)$  resonance can be clearly be seen.

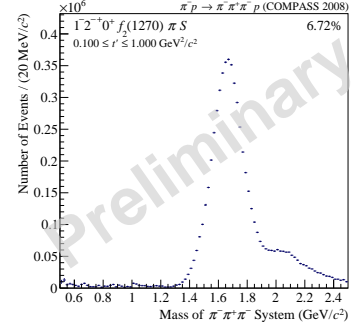


**Figure 7:** Intensity of the  $2^{-+}0^+$   $f_2(1270) \pi S$  wave. The  $\pi_2(1690)$  resonance can be clearly be seen.

$a_1(1420)$ . The mass and width of this new resonance were determined by mass dependent fits to lie in the following ranges:

$$m_{a_1(1420)} = 1412 - 1422 \text{ MeV}, \quad (3.2)$$

$$\Gamma_{a_1(1420)} = 130 - 150 \text{ MeV}. \quad (3.3)$$

Since the  $1^{++}0^+$   $f_0(980) \pi P$  wave also shows a strong phase motion (Fig.9) with respect to other waves, the observed intensity peak (Fig.8) is identified by mass-dependent fits as a new resonance, that mainly decays via  $a_1(1420) \rightarrow f_0(980) \pi^-$ . [5, 3]

#### 4. De-isobarred PWA

Although the PWA method described above turned out to be a very powerful tool and allows insight into the hadron spectrum, it has some limitations. At the moment, the parametrizations employed for the isobars have to be known beforehand and are not determined from the data. Examples for parametrizations are the relativistic Breit-Wigners or other, more elaborated models motivated by theory. However, up to now there is no definite choice for e.g. the parametrization of the  $f_0(500)$ .

To investigate possible model bias introduced by the used isobar parametrizations, a new method was introduced, called 'de-isobarring'.

##### 4.1 De-isobarring

In order to circumvent the need to put the isobar shapes into the PWA fit, de-isobarring replaces them by a set of piecewise constant functions. These functions cover the whole allowed range for  $m_{\pi^- \pi^+}$  and each of the single steps behaves like an independent partial wave with well-defined quantum numbers.

A usual PWA fit, with fixed parametrizations in the two-pion mass  $m_{\pi^- \pi^+}$ , returns one complex parameter for each wave that describes the strength and relative phase of the respective partial wave. In the de-isobarred fit, such a complex parameter is returned for every single  $m_{\pi^- \pi^+}$  bin.

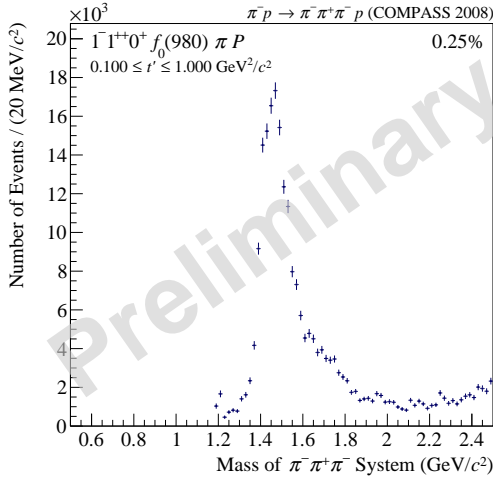


**Figure 8:** Intensity of the  $1^{++}0^+ f_0(980) \pi P$  wave. The new  $a_1(1420)$ -resonance can be clearly be seen.

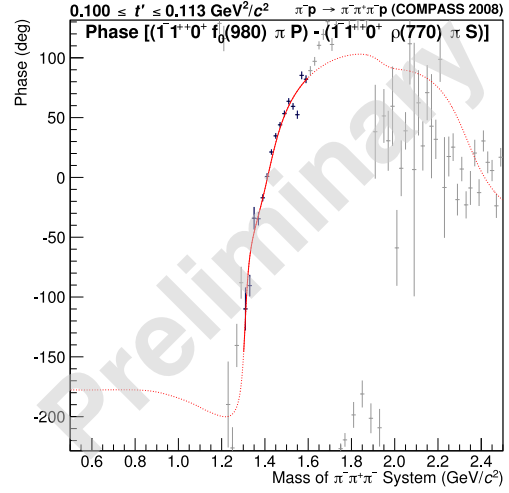


**Figure 9:** PWA results for the phase difference between the  $1^{++}0^+ f_0(980) \pi P$  wave with the  $a_1(1420)$  and the  $1^{++}0^+ \rho(770) \pi S$  wave with the  $a_1(1260)$ . A clear phase motion is visible in the region around 1.420 GeV, thus identifying the observed peak in the intensity as a resonance. The red line shows the result of a mass-dependent fit.

Since each of these steps corresponds to a certain bin in  $m_{\pi^- \pi^+}$ , the complex amplitude of the isobar can be obtained this way from these parameters as a function of  $m_{\pi^- \pi^+}$ . Since this analysis is independently performed in  $m_{3\pi}$  bins, a two-dimensional picture of the amplitude is obtained.

At the moment this procedure is applied to isoscalar  $0^{++}$  isobars, which are all replaced by the piecewise constant functions, which are henceforth denoted by  $[\pi\pi]_S^*$ :

$$[\pi\pi]_S, f_0(980), f_0(1500) \rightarrow [\pi\pi]_S^*. \quad (4.1)$$

In the present analysis, steps of 10 MeV width are used in the region from  $m_{\pi^- \pi^+} = 920$  to 1080 MeV, which is the area of the  $f_0(980)$ . Outside this range, steps of 40 MeV width were chosen, resulting in a total of 62 steps over the whole  $m_{\pi^- \pi^+}$  range which extends from  $2m_\pi$  to  $m_{3\pi} - m_\pi$ .

At the moment, the following seven partial waves were replaced by the de-isobarred  $[\pi\pi]_S^*$  waves:

Established PWA	De-isobarred PWA
$0^{-+}0^+ [\pi\pi]_S \pi S$	
$0^{-+}0^+ f_0(980) \pi S$	$0^{-+}0^+ [\pi\pi]_S^* \pi S$
$0^{-+}0^+ f_0(1500) \pi S$	
$1^{++}0^+ [\pi\pi]_S \pi P$	
$1^{++}0^+ f_0(980) \pi P$	$1^{++}0^+ [\pi\pi]_S^* \pi P$
$2^{-+}0^+ [\pi\pi]_S \pi D$	
$2^{-+}0^+ f_0(980) \pi D$	$2^{-+}0^+ [\pi\pi]_S^* \pi D$

while all other waves are still treated as in the normal PWA, with given isobar-parametrizations.

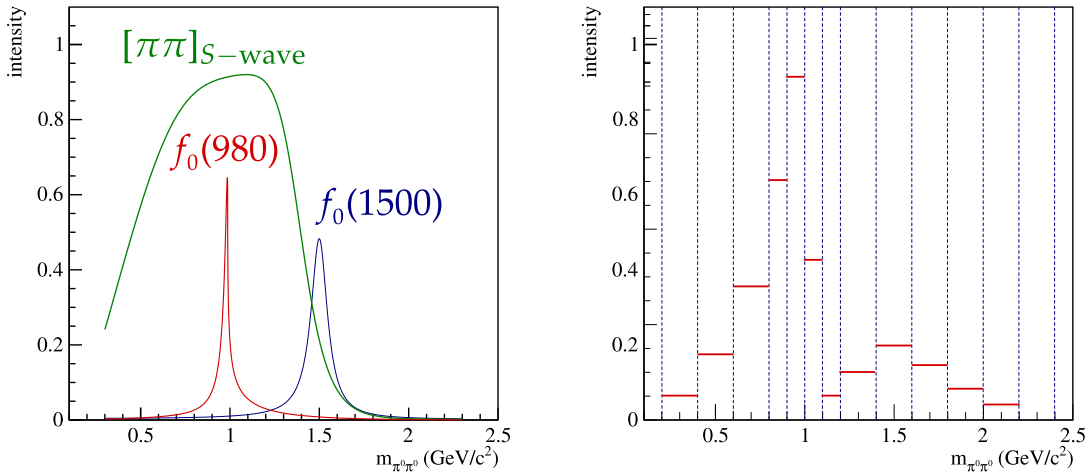


**Figure 10:** In the usual PWA (left plot), given isobar shapes are put into the fit. For  $0^{++}$  these are the  $[\pi\pi]_S$ , the  $f_0(980)$  and the  $f_0(1500)$ . For each of these isobars, one complex parameter is obtained. In the de-isobarred PWA (right plot), piecewise constant functions replace the given parametrizations and each step acts like a single isobar. A complex parameter is obtained for each of these steps, which then give the complex shape of the isobar as function of  $m_{\pi^-\pi^+}$ . In contrast to the picture above, which is just for illustration, the binning in  $m_{\pi^-\pi^+}$  is finer in actual fits.

#### 4.2 Results of the de-isobarred PWA

Performing a de-isobarred fit for the  $0^{-+}0^+$   $[\pi\pi]_S^* \pi$   $S$  wave, around a three pion mass of  $m_{3\pi} = 1.80\text{GeV}$ , the intensity and phase distributions depicted in Fig.11 and 12 are obtained for the  $\pi^- \pi^+$  system.

As in the normal PWA, this fit can be performed over the whole range of  $m_{3\pi}$  from 1.1 to 2.0GeV, which then results in a two-dimensional intensity distribution, depending on  $m_{3\pi}$  and  $m_{\pi^-\pi^+}$  (Fig.13).

In the de-isobarred fit for the  $1^{++}0^+$   $[\pi\pi]_S^* \pi$   $P$  wave a clear signal for the new  $a_1(1420)$  decaying into  $f_0(980) \pi$  (Figs.14 and 15).

The fit for the  $2^{-+}0^+$   $[\pi\pi]_S^* \pi$   $D$  wave shows the  $\pi_2(1880)$  resonance decaying into  $f_0(980) \pi$  (Figs.16 and 17).

The red lines appearing in Figs. 11, 14 and 16 correspond to phase-space integrals. Since all the shown intensities from the de-isobarred analysis are Breit-Wigner intensities, which do not contain any phase-space effects, they have to be multiplied with the integrals to obtain the number of events. This suppresses the strong enhancement at the phase-space borders seen in the  $2^{-+}0^+$   $[\pi\pi]_S^* \pi$   $D$  wave.

### 5. Conclusion

The huge data set of 50 million accepted events taken by COMPASS for three diffractively produced charged pions allows for a detailed partial-wave analysis of the  $\pi^- \pi^+ \pi^-$  final state. In this PWA, 87 different waves up to spin 6 were included.

In the present analysis, a new resonance, the  $a_1(1420)$ , was seen in the  $1^{++}0^+$   $f_0(980) \pi$   $P$  wave for the first time.

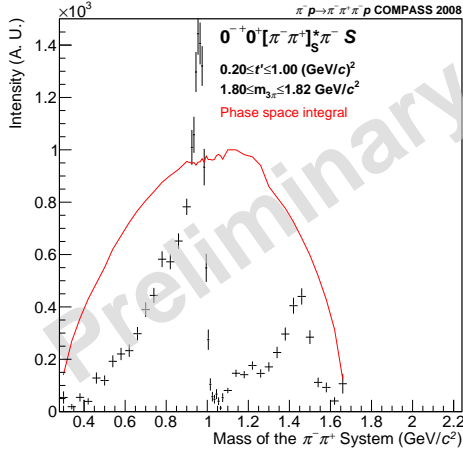


**Figure 11:** Intensity of  $0^{-+}0^{+} [\pi\pi]_S^* \pi S$  at  $m_{3\pi} = 1.80 \text{ GeV}$  as a function of  $m_{\pi^- \pi^+}$ . The  $f_0(980)$  and the  $f_0(1500)$  can be seen. Also a broad low-mass structure corresponding to the  $[\pi\pi]_S$  is visible.

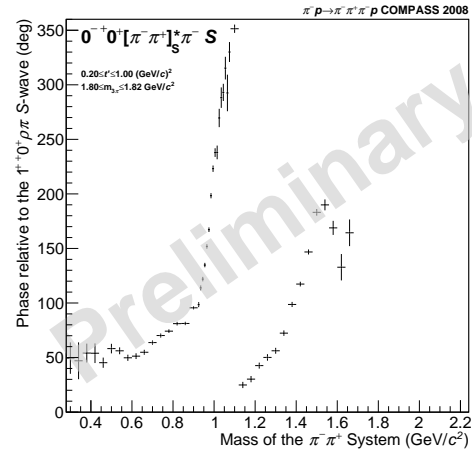


**Figure 12:** The phase diagram for  $0^{-+}0^{+} [\pi\pi]_S^* \pi S$  at  $m_{3\pi} = 1.80 \text{ GeV}$  shows strong phase motions with  $m_{\pi^- \pi^+}$ , corresponding to the  $f_0(980)$  and  $f_0(1500)$  resonances, respectively.

The large amount of data permits to apply a new PWA method, the so-called de-isobarring, which allows to extract not only the shape of three-pion waves, but also the shapes of their two-pion subsystems. This method was used to study the isoscalar  $0^{++}$  isobars and revealed rich structures for the  $0^{-+}0^{+} [\pi\pi]_S^* \pi S$ , the  $1^{++}0^{+} [\pi\pi]_S^* \pi P$  and the  $2^{-+}0^{+} [\pi\pi]_S^* \pi D$  waves. In the  $1^{++}0^{+} [\pi\pi]_S^* \pi P$  wave, the new  $a_1(1420)$  is also visible, so it is very likely not an artifact of the isobar parametrizations used for  $[\pi\pi]_S$ ,  $f_0(980)$  and  $f_0(1500)$ .

## 6. Outlook

As next steps, mass-dependent fits on the results of the PWA, normal and de-isobarred, have to be performed in order to finally extract the resonance parameters.

Also, the de-isobarred PWA will be extended to isobars with  $J^{PC} \neq 0^{++}$ , e.g. to isobars with  $J^{PC} = 1^{--}$  or  $2^{++}$ , which correspond to the  $\rho(770)$  and the  $f_2(1270)$ , respectively, possibly plus their respective excited states. This will give new insight into the  $[\pi\pi]_P^*$  and  $[\pi\pi]_D^*$  wave as well.

## References

- [1] J. Beringer *et al.* [Particle Data Group Collaboration], Phys. Rev. D **86** (2012) 010001.
- [2] K. L. Au, D. Morgan and M. R. Pennington, Phys. Rev. D **35** (1987) 1633.
- [3] S. Paul [for the COMPASS Collaboration], EPJ Web of Conference 2013 [arXiv:1312.3678 [hep-ex]].
- [4] B. Ketzner [for the COMPASS Collaboration], arXiv:1403.4884 [hep-ex].
- [5] S. Uhl [on behalf of the COMPASS Collaboration], arXiv:1401.4943 [hep-ex].

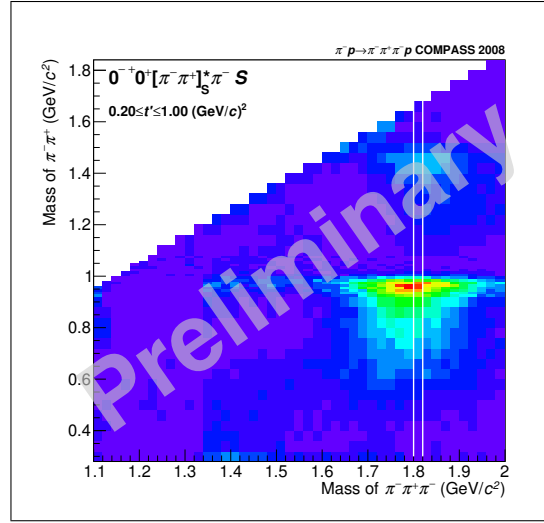


**Figure 13:** Intensity of the  $0^{-+}0^{+} [\pi\pi]_S^* \pi S$  wave as a function of the two- and three-pion mass. A strong correlation between  $2\pi$ - and  $3\pi$ -structures is visible. The most prominent peak corresponds to the decay of the  $\pi(1800)$  resonance into  $f_0(980) \pi^-$ . The decay  $\pi(1800) \rightarrow f_0(1500) \pi$  is also visible. The white lines indicate the position of the slice shown above.

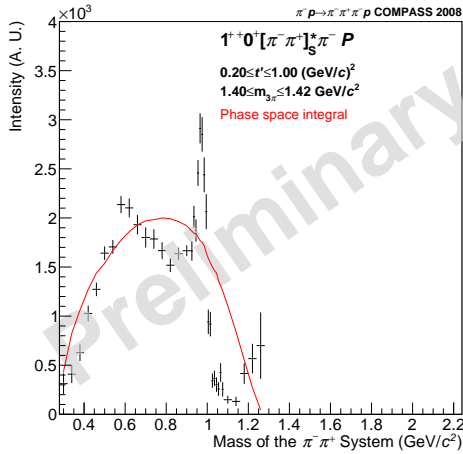


**Figure 14:** Intensity of the  $1^{++}0^{+} [\pi\pi]_S^* \pi P$  wave at  $m_{3\pi} = 1.40 \text{ GeV}$  as a function of  $m_{\pi^- \pi^+}$ . The  $f_0(980)$  can be seen. Also a broad low-mass structure corresponding to the  $[\pi\pi]_S$  is visible.

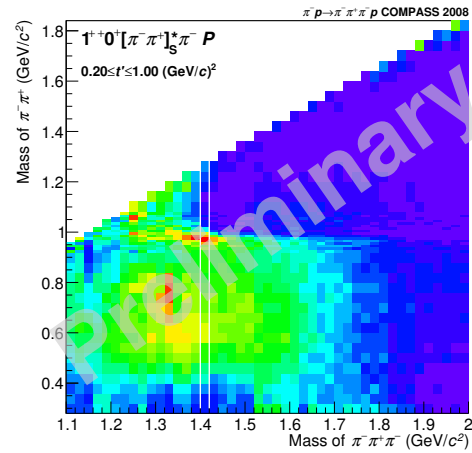


**Figure 15:** The two-dimensional intensity distribution shows a broad structure for lower  $m_{3\pi}$  correlated with the broad  $[\pi\pi]_S$ . A clear peak for  $a_1(1420) \rightarrow f_0(980) \pi$  is also visible.

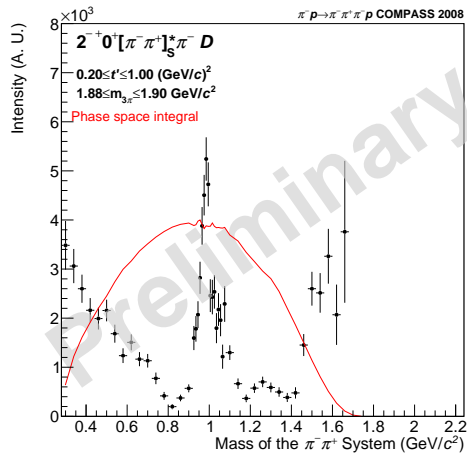


**Figure 16:** Intensity of the  $2^{-+}0^{+} [\pi\pi]_S^* \pi D$  wave at  $m_{3\pi} = 1.88\text{GeV}$  as a function of  $m_{\pi^- \pi^+}$ . The  $f_0(980)$  can be seen.

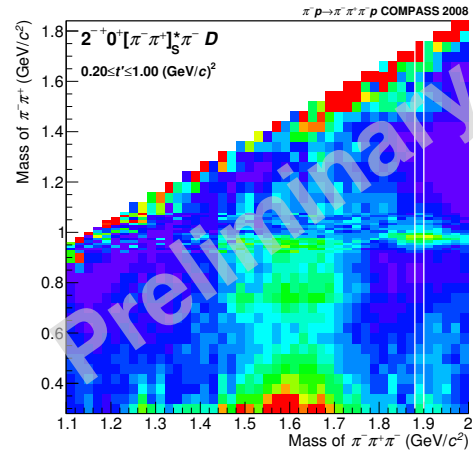


**Figure 17:** The two-dimensional intensity shows a peak for  $\pi_2(1880) \rightarrow f_0(980) \pi$ .